
JAAS
Journal of Analytical Atomic Spectrometry
Hg
Pb
Fe

Temporal Changes of Size Distribution of Mass and Relative Intensity for Ablated Particles during Laser Ablation Inductively Coupled Plasma Mass Spectrometry

Ryo MACHIDA, Takashi NAKAZAWA, and Naoki FURUTA*

Faculty of Science and Engineering, Department of Applied Chemistry, Chuo University, 1-13-27 Kasuga, Bunkyo-ku, Tokyo 112-8551, Japan

*To whom correspondence should be addressed.

E-mail address: nfuruta@chem.chuo-u.ac.jp

Tel & Fax: +81-3-3817-1906

Abstract

To investigate elemental fractionation during laser ablation–inductively coupled plasma mass spectrometry (LA-ICPMS) we measured mass fractions of ablated particles and chemical composition of ablated particles in this study. Temporal changes of fractionation index (FI) were investigated under laser defocus conditions which caused a large variation of size distribution of abated particles. It was a useful technique for understanding relationship between temporal changes of FI and the size of ablated particles. Ablated particles were fractionated by aerodynamic diameter (<0.06, 0.06–0.22, 0.22–2.2, and >2.2 μm) with a low-pressure impactor and were digested with HNO_3 and HF; then As, Rb, Rh, La, Gd, Yb, W, Re, and Th were measured by ICPMS. Under 0.5 mm defocus and 1.0 mm defocus conditions, the mass fractions (ablated particle mass at 1-5 min divided by that at 0-1 min) of ablated particles larger than 0.22 μm were larger than the mass fractions of ablated particles smaller than 0.22 μm. Volatile elements such as As and Rb were enriched in particles smaller than 0.22 μm, owing to the large aspect ratio of the crater under defocus conditions. However, the magnitude of the enrichment for volatile elements did not change as ablation progressed. Therefore, we concluded that large particles could not be decomposed completely in the ICP and the FI peak observed at 2–3 min was caused by changes in elemental behavior due to changes in ablated particles larger than 0.22 μm.

1. Introduction

Laser ablation–inductively coupled plasma mass spectrometry (LA-ICPMS) is an effective technique for multielemental analysis of solid samples. However, LA-ICPMS suffers from elemental fractionation, whereby elements in a sample are enriched (or depleted) during the laser ablation process and in the plasma, to an extent that depends on the elemental properties.[1–4] The fractionation mechanism has not been definitively elucidated.[5–8] Elemental fractionation can be quantified in terms of the fractionation index (FI).[9–11] Temporal changes of FI were investigated under laser defocus conditions. When laser ablation was performed under defocus conditions, a large variation of diameter of ablated particles was observed. It was a useful technique for understanding relationship between temporal changes of FI and the size of ablated particles. We previously reported that temporal changes in FI were caused by changes in elemental behavior resulting from changes in ablated particles with aerodynamic diameters (Dp) larger than 2.0 μm introduced into the ICP, which could not be decomposed completely in the ICP.[1] However, the variation of FI for smaller ablated particles and the chemical composition of fine particles have not been sufficiently investigated. Koch *et al.* studied the particle size distributions and composition of a brass sample.[12] In the current study, we used NIST 610 glass standard material as a sample. Four fractions of size-classified ablated particles (Dp values of <0.06, 0.06–0.22, 0.22–2.2, and >2.2 μm) were collected on filters and digested with HNO_3 and HF, and then the elements in the particles were determined by ICPMS. Elemental fractionation is discussed on the basis of the size distribution of mass and the relative intensity of metal and ytterbium.

2. Experimental

2.1 Instrumentation

A laser ablation system (UP-213, ESI, Portland, OR, USA) combined with an ICPMS instrument (Agilent 7500ce, Agilent Technologies, Tokyo, Japan) was used to analyze a NIST 610 (National Institute of Standards and Technology, Maryland, USA) glass standard sample. The beam shape of the laser system was flat top shape under in focus condition. Commercially available a large-format (15 sq. cm) laser ablation cell (ESI, Portland, OR, USA) was used. To reduce wash-out time, a quartz ring with a volume of approximately 0.8 cm^3 was put inside the large-format cell. Laser ablation was carried out in a He atmosphere, and the ablated particles were introduced into a cascade impactor (inline type with NL-1-1A (<1.0 μm), Tokyo Dylec, Tokyo, Japan), which removes ablated particles larger than 1.0 μm. Ar gas was introduced between the large-format cell and the cascade impactor. The LA-ICPMS measurement conditions used in this study are summarized in Table 1. In focus, 0.5 mm defocus, and 1.0 mm defocus conditions were used to evaluate the effects of defocus conditions. These three focus condition was selected as typical trends of temporal changes of FIs. Under -1.0 mm defocus and 1.5 mm defocus condition, no signal was observed by LA-ICPMS. Temporal changes of FIs under -0.5 mm defocus condition showed the same trend as those under in focus condition.

An optical microscope (VHX-2000, Keyence, Osaka, Japan) was used for detailed observation of the crater. Crater diameter and depth were measured by observing the sample from top and from side, respectively, after laser irradiation under in focus, 0.5 mm defocus, and 1.0 mm defocus conditions. When laser ablation was performed for 10 min, 12000 shots (20 Hz × 600 sec) of laser pulse were irradiated on the sample surface. The crater diameters were 100, 60, and 200 μm, respectively, and the crater depths were

380, 1500, and 1600 µm, respectively. Shapes of the craters were top hat shape under in focus condition and a reverse circular cone under defocus conditions.

2.2 Reagents

HF (25 M, Daikin Industries, Osaka, Japan) and HNO_3 (ultrapure, 11 M, Kanto Chemical, Tokyo, Japan) were used for acid digestion. Calibration standard solutions were prepared from the following SPEX CertiPrep (Metuchen, NJ, USA) multielement standards for ICPMS: XSTC-1, XSTC-8, and XSTC-13. The standards were diluted with 0.1 M HNO_3. Calibration curves were prepared by measurement of standard solutions at concentrations of 0, 10, 100, 500, and 5000 pg mL^{-1}.

2.3 Collection of size-classified ablated particles with a low-pressure impactor

Four fractions of size-classified ablated particles (Dp values of <0.06, 0.06–0.22, 0.22–2.2, and >2.2 µm) were collected by means of a low-pressure impactor (LP-20; Tokyo Dylec Co., Tokyo, Japan), which was placed in an ISO class 4 clean bench equipped with HEPA filters (Fig. 1). Particle fractions were collected on PTFE filters (T010A080C, 80 mm diameter, Advantec Toyo Kaisya, Tokyo, Japan), except for the finest fraction (<0.06 µm), which was collected on a quartz fiber filter (2500 QAT-UP; 80 mm diam., Pall Corporation, Port Washington, NY, USA).

2.4 Acid digestion

The collected particles were decomposed with a mixture of 25 M HF (0.3 mL) and 11 M HNO_3 (0.6 mL) at 180 °C on a hotplate. Heating continued until the HF had evaporated completely and the digested solution became to one droplet. Then, the digested solution was diluted to 2 mL with 0.1 M HNO_3. As an internal standard 20 ng of Rh was added into the samples.

3. Results and discussion

3.1 Fractionation index obtained by means of LA-ICPMS with a cascade impactor

Using the single-site mode under in focus, 0.5 mm defocus, and 1.0 mm defocus conditions, we measured the elemental intensities of As and Ca by means of time-resolved analysis. In the previous paper,[1] 34 elements were classified into two groups in accordance with their observed temporal changes of FIs. Elements in the first group (Group 1) showed the FI peak at 2-3 min after the start of laser ablation under defocus conditions. Volatile elements such as As include in the first group. Elements in the second group (Group 2) did not show the FI peak as laser ablation progressed. Non-volatile elements such as Ca include in the second group. For this set of experiments, As was selected as a typical element of the first group of elements. The signal intensities and FIs for As as a function of ablation time are shown in Fig. 2.

Under the in focus condition, the plot of FI for As did not show a peak at an ablation time of 2–3 min, whereas a peak in FI was observed at 2–3 min under the 0.5 mm defocus and 1.0 mm defocus conditions (Fig. 2d–f). The magnitudes of the FI peaks were 2.3 without the 1.0 μm impactor and 1.9 with the impactor under the 0.5 mm defocus condition. Under the 1.0 mm defocus condition, the corresponding magnitudes were 1.9 and 1.4, respectively. That is, although the FI peak was suppressed by the use of the impactor, the peak did not disappear completely.

3.2 Mass of size-classified ablated particles collected with a low-pressure impactor

The size-classified ablated particles were collected on different filters by means of the low-pressure impactor sampler. The particle fractions were decomposed with acid, and ICPMS was used to determine Yb, which was suitable for estimation of the mass of ablated particles because the background was low and the sensitivity was high for ICPMS measurement. Moreover, Yb is typical for the elements classified as Group 2 in our previous study.[1] The mass of ablated particles was calculated from the mass of Yb by dividing by the certified value for Yb (473 μg g^{-1}) in the NIST 610 glass standard. A mass fraction was calculated by dividing the mass of ablated particles at 1-5 min by the mass of ablated particles at 0-1 min.

The masses of ablated particles and the mass fractions of the size-classified ablated particles are shown in Fig. 3. The total masses of ablated particles collected at 0-1 min of ablation under in focus, 0.5 mm defocus, and 1.0 mm defocus conditions were 15.2, 10.2, and 8.8 pg, respectively, and the total masses of ablated particles collected at 1-5 min under in focus, 0.5 mm defocus, and 1.0 mm defocus conditions were 5.1, 3.6, and 3.2 pg, respectively. The ratios of the total masses collected at 1-5 min to the total masses collected at 0-1 min of ablation were 34%, 35%, and 36% under in focus, 0.5 mm defocus, and 1.0 mm defocus conditions, respectively. Under the defocus conditions, the mass fractions of particles larger than 0.22 μm were high: specifically, 57% (0.22–2.2 μm) and 59% (>2.2 μm) under the 0.5 mm defocus condition and 54% (0.22–2.2 μm) and 51% (>2.2 μm) under the 1.0 mm defocus condition. These results confirm that the mass of particles larger than 0.22 μm was higher at 1–5 min than at 0–1 min when laser ablation was performed under defocus conditions.

Smaller particles (<0.06 μm) were produced in greater amounts than larger particles. However, under all three focus conditions, the mass fractions of these smaller particles were the same as the ratios of the total masses collected at 1-5 min to the total masses collected at 0-1 min of ablation. The mass fractions of the larger particles increased under defocus conditions. Therefore, we concluded that the FI peak at 2–3 min was caused by changes in ablated particles larger than 0.22 μm.

3.3 Chemical composition of size-classified ablated particles

The amounts of As, Rb, Re, W, La, Gd, Th, and Yb in the size-classified ablated particles were determined by means of ICPMS, and temporal FIs were calculated from Eq. (1):

$$\text{temporal FI} = \left[\frac{(M/Yb)_{\text{1-5 min}}}{(M/Yb)_{\text{0-1 min}}}\right] \qquad \text{Eq.(1)}$$

where $(M/Yb)_{1\text{-}5\ min}$ is the relative intensity of element M normalized by the signal intensity of Yb at 1-5 min of ablation, and $(M/Yb)_{0\text{–}1\ min}$ is the relative intensity of element M normalized by the signal intensity of Yb at 0-1 min of ablation. The relative intensities and temporal FIs of all the elements, along with the melting points (mp) of their oxides, are listed in Table 2. The temporal FIs of the first group of elements (Group 1) were between 0.8 and 1.2 and those of the second group of elements (Group 2) were between 0.9 and 1.1. All the FIs were approximately 1 and did not depend on the size of the ablated particles, indicating that the magnitude of the enrichment did not change as laser ablation progressed.

The crater aspect ratios under in focus (11 J cm^{-2}), 0.5 mm defocus (30 J cm^{-2}), and 1.0 mm defocus (3.0 J cm^{-2}) conditions were 3.8, 25, and 8.0, respectively. The fluence was calculated from the diameter of the crater produced on the sample surface. The actual fluence increased as laser ablation progressed. For the elemental composition, the relative intensities of As in the particles smaller than 0.06 μm at 0-1 min of ablation under in focus, 0.5 mm defocus, and 1.0 mm defocus conditions were 0.08, 0.20, and 0.13, respectively. The corresponding values for Rb were 1.53, 2.73, and 1.81. The relative intensities of the volatile elements under 0.5 mm defocus condition were larger than those under in focus and 1.0 mm defocus conditions. However, the relative intensities of the elements in Group 2 were constant regardless of the focus conditions. The relative intensities of volatile elements increased as the aspect ratio of the crater increased. The relative intensities of As at 0-1 min of ablation under 0.5 mm defocus condition were 0.20, 0.17, 0.09, and 0.11 for particles with sizes of <0.06, 0.06–0.22, 0.22–2.2, and >2.2 μm, respectively. The relative intensities of As in particles smaller than 0.22 μm were larger than those of As in particles larger than 0.22 μm. The same trend was observed for Rb. We confirmed that during laser ablation, elemental fractionation varied with aspect ratio.[13] Volatile elements were enriched in smaller particles because smaller particles were generated by hydrodynamic sputtering in the heat-effective zone on the sample surface. The size dependence of the chemical composition of the particles was caused by noncongruent evaporation.[14–16]

However, the relative intensities of elements in Group 1 at 1-5 min of ablation were the same as those observed at 0-1 min of ablation. That is, the magnitude of the enrichment of the elements in Group 1 at 0-1 min of ablation was the same as that at 1-5 min of ablation. This result indicates that the FI peak observed for elements in Group 1 at 2–3 min after the start of laser ablation was caused not by smaller particles but by particles larger than 0.22 μm. Particles larger than 0.22 μm could not be decomposed completely in the ICP and elements in Group 1 were more easily vaporized and ionized than Ca.

4. Conclusions

In this study, ablated particles were classified by size, and the chemical composition of the particles was investigated. The FI peak observed for elements in Group 1 under defocus conditions at 2–3 min after the start of laser ablation was suppressed by the use of a 1.0 μm impactor, but the peak did not disappear completely. Under the in focus condition, the mass fraction of ablated particles did not change. In contrast, under 0.5 mm defocus and 1.0 mm defocus conditions, the mass fraction of ablated particles increased for ablated particles larger than 0.22 μm.

Volatile elements were enriched in small particles produced during laser ablation regardless of the focus conditions. The magnitude of the enrichment increased as the aspect ratio of the crater increased. However, the magnitude of the enrichment at 0-1 min of ablation was the same as that at 1-5 min of ablation. These experimental results indicate that the FI peak observed for Group 1 elements under defocus conditions at 2–3 min after the start of ablation was caused not by smaller particles but by particles larger than 0.22 μm. Particles larger than 0.22 μm could not be decomposed completely in the ICP and elements in Group 1 were more easily vaporized and ionized than Ca.

5. Acknowledgements

This research was supported by the Ministry of Education, Culture, Sports, Science and Technology, Japan, through a Grant-in-Aid for Scientific Research (C) (no. 26410160) and a Grant-in-Aid for Young Scientists (B) (no. 26870595). Part of this study was supported under a joint research project conducted at the Institute of Science and Engineering of Chuo University.

References

1. R. Machida, T. Nakazawa, and N. Furuta, *Anal. Sci*., 2015, **31**, 345-355.
2. R. E. Russo, X. Mao, J. J. Gonzalez, V. Zorba, and J. Yoo, *Anal. Chem.*, **2013**, 85, 6162-6177.
3. R. E. Russo, X. Mao, H. Liu, J. Gonzalez, and S. S. Mao, *Talanta*, 2002, **57**, 425–451.
4. H. P. Longerich, D. Günther, and S. E. Jackson, *Fresenius J. Anal. Chem.*, **1996**, 355, 538-542.
5. D. Günther and C. A. Heinrich, *J. Anal. At. Spectrom.*, **1999**, 14, 1369-1374.
6. Z. Wang, B. Hattendorf, and D. Günther, *J. Am. Soc. Mass Spectrom.*, **2006**, 17, 641-651.
7. C. Liu, X. L. Mao, S. S. Mao, X. Zeng, R. Greif, and R. E. Russo, *Anal. Chem.*, **2004**, 76, 379-383.
8. T. Hirata and Y. Kon, *Anal. Sci.*, **2008**, 24, 345-353.
9. I. Kroslakova and D. Günther, *J. Anal. At. Spectrom*., 2007, **22**, 51-62.
10. T. E. Jeffries, S. E. Jackson, and H. P. Longerich, *J. Anal. At. Spectrom*., 1998, **13**, 935-940.
11. M. Ohata, D. Tabersky, R. Glaus, J. Koch, B. Hattendorf, and D. Günther, *J. Anal. At. Spectrom*., 2014, **29**, 1345-1353.
12. J. Koch, A. von Bohlen, R. Hergenröder and K. Niemax, *J. Anal. At. Spectrom*., 2004, **19**, 267-272.
13. O. V. Borisov, X. Mao, and R. E. Russo, *Spectrochim. Acta, Part B: At. Spectrosc.*, 2000, **55**, 1693-1704.
14. R. Hergenröder, *J. Anal. At. Spectrom*., 2006, **21**, 505-516.

15. H. R. Kuhn and D. Günther, *J. Anal. At. Spectrom.*, 2004, **19**, 1158-1164.

16. R. Machida, T. Nakazawa, Y. Sakuraba, M. Fujiwara, and N. Furuta, *J. Anal. At. Spectrom.*, 2015, **30**, 2412-2419.

Table 1 Operating conditions used for laser ablation and ICPMS measurements

Laser Ablation		
Laser model	UP213	
Laser type	Nd:YAG	
Wavelength	213 nm	
Pulse width	4 ns	
Ablation mode	Single site	
Repetition rate	20 Hz	
Carrier gas (He) flow rate	1.0 L min^{-1}	
Laser energy on sample surface	0.9 mJ	
Initial laser fluence*		
In focus	11 J cm^{-2}	
0.5 mm defocus	30 J cm^{-2}	
1.0 mm defocus	3.0 J cm^{-2}	
Crater diameter		
In focus	100 ± 5 μm	
0.5 mm defocus	60 ± 4 μm	
1.0 mm defocus	200 ± 10 μm	
Crater depth		
In focus	380 ± 30 μm	
0.5 mm defocus	1500 ± 150 μm	
1.0 mm defocus	1600 ± 150 μm	
ICPMS Measurements		
ICPMS model	Agilent 7500cc	
RF power	1600 W	
Integration time	0.05 s	
Collision gas (He) flow rate	2.0 mL min^{-1}	
	for laser ablation	for solution nebulization
Carrier gas (Ar) flow rate	0.8 L min^{-1}	1.2 L min^{-1}
Sample uptake rate	-	0.1 mL min^{-1}
Isotopes measured	^{42}Ca, ^{75}As	^{75}As, ^{85}Rb, ^{103}Rh, ^{139}La, ^{157}Gd, ^{173}Yb, ^{182}W, ^{185}Re, ^{232}Th

* Actual fluence changed with time.

Table 2 Relative intensity data for size-classified particles and temporal FIs of elements along with melting points of their oxides

			Aerodynamic diameter under in focus conditions											
			<0.06 µm			0.06-0.22 µm			0.22-2.2 µm			>2.2 µm		
		mp of oxide	Relative intensity		temporal FI	Relative intensity		temporal FI	Relative intensity		temporal FI	Relative intensity		temporal FI
Group*	Element	(°C)	$(M/Yb)_{0-1}$	$(M/Yb)_{1-5}$		$(M/Yb)_{0-1}$	$(M/Yb)_{1-5}$		$(M/Yb)_{0-1}$	$(M/Yb)_{1-5}$		$(M/Yb)_{0-1}$	$(M/Yb)_{1-5}$	
1	As	274	0.08	0.09	1.1 ± 0.2	0.04	0.05	1.1 ± 0.2	0.04	0.05	1.1 ± 0.2	0.06	0.05	1.0 ± 0.2
1	Rb	412	1.53	1.66	1.1 ± 0.0	0.84	0.94	1.1 ± 0.1	0.87	0.77	0.9 ± 0.1	0.99	0.96	1.0 ± 0.2
1	Re	900	0.19	0.17	0.9 ± 0.1	0.15	0.17	1.1 ± 0.1	0.15	0.15	1.0 ± 0.2	0.18	0.16	0.9 ± 0.2
1	W	1500	1.01	0.90	0.9 ± 0.1	0.88	0.92	1.0 ± 0.1	0.94	0.76	0.8 ± 0.2	0.90	0.85	0.9 ± 0.0
2	La	2315	3.47	3.51	1.0 ± 0.1	3.34	3.53	1.1 ± 0.1	3.45	3.37	1.0 ± 0.0	3.79	3.36	0.9 ± 0.1
2	Gd	2339	0.75	0.76	1.0 ± 0.2	0.72	0.77	1.1 ± 0.1	0.72	0.73	1.0 ± 0.0	0.82	0.80	1.0 ± 0.4
2	Th	3390	3.00	2.64	0.9 ± 0.1	3.41	3.48	1.0 ± 0.0	3.45	3.47	1.0 ± 0.0	3.39	3.38	1.0 ± 0.0

			Aerodynamic diameter under 0.5 mm defocus conditions											
			<0.06 µm			0.06-0.22 µm			0.22-2.2 µm			>2.2 µm		
		mp of oxide	Relative intensity		temporal FI	Relative intensity		temporal FI	Relative intensity		temporal FI	Relative intensity		temporal FI
Group*	Element	(°C)	$(M/Yb)_{0-1}$	$(M/Yb)_{1-5}$		$(M/Yb)_{0-1}$	$(M/Yb)_{1-5}$		$(M/Yb)_{0-1}$	$(M/Yb)_{1-5}$		$(M/Yb)_{0-1}$	$(M/Yb)_{1-5}$	
1	As	274	0.20	0.22	1.1 ± 0.1	0.17	0.20	1.2 ± 0.2	0.09	0.09	1.0 ± 0.3	0.11	0.10	0.9 ± 0.2
1	Rb	412	2.73	2.60	1.0 ± 0.3	1.68	1.70	1.0 ± 0.2	0.91	0.80	0.9 ± 0.1	0.96	0.95	1.0 ± 0.2
1	Re	900	0.16	0.16	1.0 ± 0.2	0.36	0.37	1.0 ± 0.2	0.17	0.15	0.9 ± 0.2	0.11	0.10	0.9 ± 0.3
1	W	1500	1.47	1.47	1.0 ± 0.1	1.97	2.15	1.1 ± 0.2	1.14	1.03	0.9 ± 0.1	1.14	1.12	1.0 ± 0.3
2	La	2315	3.73	3.42	0.9 ± 0.1	3.90	3.73	1.0 ± 0.1	3.37	3.43	1.0 ± 0.1	2.89	3.02	1.0 ± 0.1
2	Gd	2339	0.84	0.88	1.1 ± 0.1	0.79	0.75	0.9 ± 0.1	0.68	0.63	0.9 ± 0.1	0.77	0.77	1.0 ± 0.3
2	Th	3390	2.73	2.88	1.1 ± 0.1	3.01	3.01	1.0 ± 0.0	2.85	2.75	1.0 ± 0.1	2.65	2.81	1.1 ± 0.3

			Aerodynamic diameter under 1.0 mm defocus conditions											
			<0.06 µm			0.06-0.22 µm			0.22-2.2 µm			>2.2 µm		
		mp of oxide	Relative intensity		temporal FI	Relative intensity		temporal FI	Relative intensity		temporal FI	Relative intensity		temporal FI
Group*	Element	(°C)	$(M/Yb)_{0-1}$	$(M/Yb)_{1-5}$		$(M/Yb)_{0-1}$	$(M/Yb)_{1-5}$		$(M/Yb)_{0-1}$	$(M/Yb)_{1-5}$		$(M/Yb)_{0-1}$	$(M/Yb)_{1-5}$	
1	As	274	0.13	0.15	1.1 ± 0.3	0.06	0.05	0.9 ± 0.1	0.06	0.05	1.0 ± 0.2	0.09	0.10	1.1 ± 0.1
1	Rb	412	1.81	1.68	0.9 ± 0.2	0.84	0.92	1.1 ± 0.2	0.84	0.81	1.0 ± 0.1	0.91	0.92	1.0 ± 0.3
1	Re	900	0.19	0.18	1.0 ± 0.2	0.16	0.17	1.1 ± 0.1	0.12	0.12	1.0 ± 0.2	0.17	0.18	1.0 ± 0.3
1	W	1500	1.04	1.15	1.1 ± 0.4	N. D.	N. D.	–	N. D.	N. D.	–	N. D.	N. D.	–
2	La	2315	3.14	3.46	1.1 ± 0.1	3.52	3.85	1.1 ± 0.1	3.51	3.69	1.1 ± 0.1	3.63	3.98	1.1 ± 0.2
2	Gd	2339	0.67	0.76	1.1 ± 0.3	0.74	0.78	1.1 ± 0.1	0.75	0.71	0.9 ± 0.1	0.77	0.81	1.1 ± 0.2
2	Th	3390	3.20	2.96	0.9 ± 0.3	3.36	3.40	1.0 ± 0.0	3.34	3.11	0.9 ± 0.1	3.27	3.62	1.1 ± 0.2

* Ref.1

Figure Captions

Fig. 1 Schematic diagram of experimental setup used to collect ablated particles on four separate filters.

Fig. 2 Signal intensities of As obtained by LA-ICPMS. Laser ablation was performed under (a) in-focus, (b) 0.5 mm defocus, and (c) 1.0 mm defocus conditions without (black) and with (gray) a 1.0 μm impactor. Fractionation indexes of As during laser ablation under (d) in-focus, (e) 0.5 mm defocus, and (f) 1.0 mm defocus conditions without (triangles) and with (circles) a 1.0 μm impactor. Error bars indicate standard deviations (n = 3).

Fig. 3 Masses of ablated particles (bars) and mass fractions of size-classified ablated particles (gray circles) obtained under (a) in focus, (b) 0.5 mm defocus, and (c) 1.0 mm defocus conditions at 0-1 min of ablation (black bars) and at 1-5 min of ablation (gray bars). Dashed lines indicate the ratios of the total masses collected at 1-5 min to the total masses collected at 0-1 min. Error bars indicate standard deviations (n = 3).

Fig. 1 Machida *et al.*

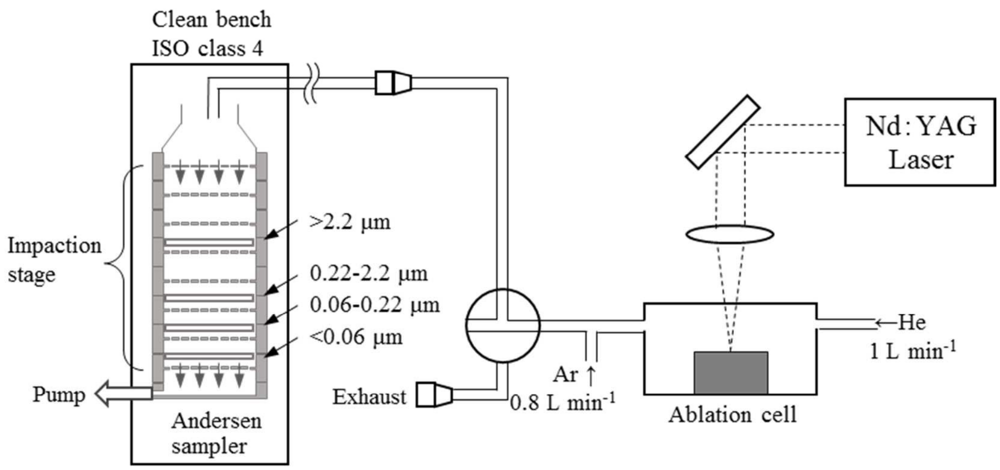

Fig. 2 Machida *et al.*

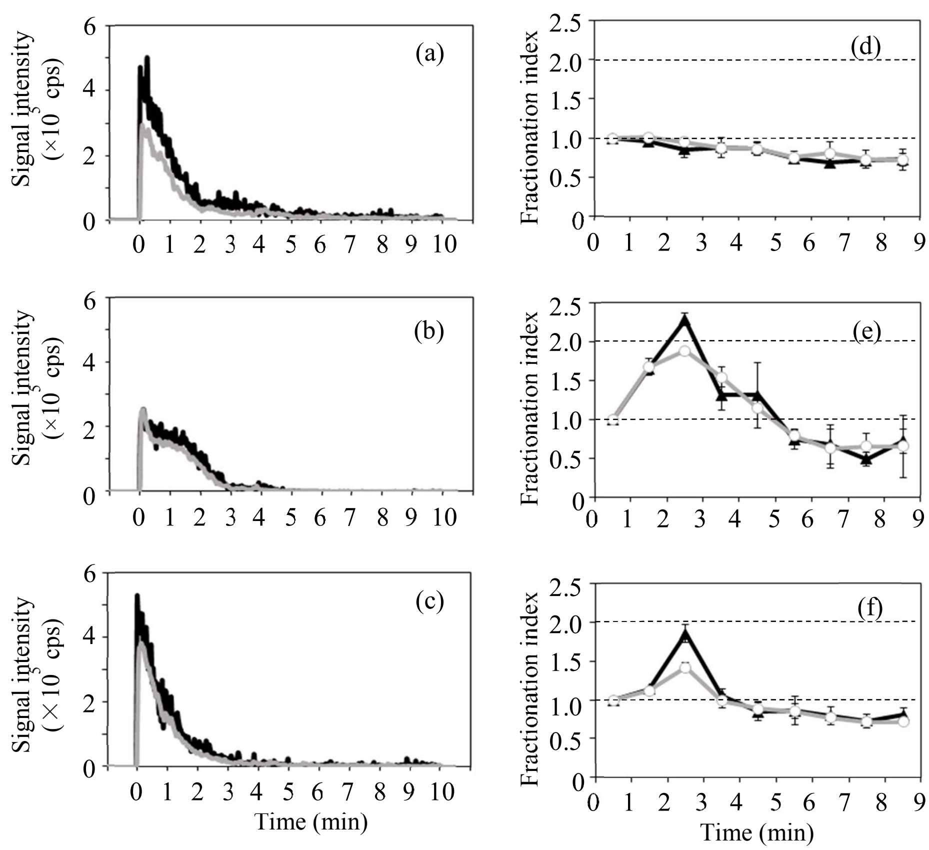

Fig. 3 Machida *et al.*